

Supplementary Material

Influence of surface heterogeneities on complexation of ethylene with active sites of NiMCM-41 nanocatalyst: a density functional theory study

Mehdi Ghambarian¹, Mohammad Ghashghaee^{2,*}, Zahra Azizi^{3,†}, Mahboobeh Balar^{3,4}

¹ *Gas Conversion Department, Faculty of Petrochemicals, Iran Polymer and Petrochemical Institute, P.O. Box 14975-112, Tehran, Iran*

² *Faculty of Petrochemicals, Iran Polymer and Petrochemical Institute, P.O. Box 14975-112, Tehran, Iran*

³ *Department of Chemistry, Karaj Branch, Islamic Azad University, P.O. Box 31485-313, Karaj, Iran*

⁴ *Young Researchers and Elite Club, Karaj Branch, Islamic Azad University, Karaj, Iran*

* Corresponding author. Tel.: +98 21 48662481; fax: +98 21 44787032. E-mail address: m.ghashghaee@ippi.ac.ir.

† Corresponding author. Tel.: +98 26 34182305; fax: +98 26 34418156. E-mail address: zahra.azizi@kiau.ac.ir, zahraazizi@yahoo.com.

Supplementary Results and Discussion

Ethylene molecules were adsorbed consecutively on 7 active sites of the model NiMCM-41 catalyst such that 14 adsorption structures were optimized, each with two computational methods. The model nanoclusters of the active sites were identified previously [1] through an exploration of a proper silica matrix for different defect sites among geminal, vicinal, and close non-vicinal silanol groups where the latter pairs were linked by two or more of siloxane bridges. As such, the models differed in terms of the size of the ring (2T–6T) or the interatomic distance between the next-nearest-neighbor silicon atoms with respect to the nickel center.

Table S1 reports the NBO partial charges and the total adsorbate charges (Q) for the optimized complexes. The corresponding data for the L1 level are listed in the supporting information (Table S5). The NBO population results indicated that the total charge of adsorptive molecules changed on average by +0.143 and +0.205 e per molecule, respectively, through monomeric and dimeric adsorption events on NiMCM-41 at the L2 level. The corresponding data with L1 were 0.107 and 0.175 e per molecule, respectively, which were smaller than those at L2. Concomitantly, the Ni partial charges were on average 0.818 and 0.637 e at L2 (and 0.893 and 0.741 e at L1), respectively, for the monomeric and dimeric adsorption structures; the partial charges were slightly smaller than those on the initially exposed Ni cations which were almost half the formal charge of +2 [1]. These observations proved that Ni²⁺ centers withdrew partial charges from adsorbate molecules; this withdrawal was interestingly more pronounced in the dimeric adsorption mode. This partial charge transfer was minimal (0.022 and 0.059 e at L1 and L2, respectively) on 2T and maximum (0.217 and 0.243 e at L1 and L2, respectively) on 4T, whether one or two molecules of ethylene were adsorbed. Correspondingly, the most and least negative charges were found on the carbon atoms of ethylene molecules adsorbed on the 2T and 4T sites, respectively.

For the monomeric adsorption mode, the lower the charge alterations in the adsorbed molecules, the more negatively charged the carbon atoms (see, e.g., the values of Q_1 and $q(=C1a)$ in Table S1). Relative to the free adsorptive molecules, however, the direction of the charge alterations on the C atoms were not concurrent. In other words, some adsorbate molecules had carbon atoms with partial charges lower than that in the free molecule (with the carbon partial charges of -0.373 and -0.364 e at L2 and L1) and some higher. No further relationship could be established between the charge trends of different elements. Moreover, the atomic charge alterations were more complicated in the case of dimeric adsorption. As also evident, the two methods treated the atomic partial charges almost similarly except for the transition metal (nickel) which subsequently affected the total adsorbate charges differently. Furthermore, Table S6 indicated that the average Mulliken atomic charges on Ni, O, and C atoms were generally 0.30, 0.41, and 0.44 times those of the NBO data, thus tending to remain closer to neutrality.

Table S2 reports a number of selected interatomic distances and the relevant bond angles for the adsorption complexes at L2, with the related data at L1 given in Table S7. The initially formed Ni–O distances ranged from 1.69 to 1.79 Å at L2 [1], which were in a reasonable agreement with the experimental values of 1.60–2.04 [2-3] for analogous nickel-incorporated silica systems. Compared to the mentioned initial Ni–O bond lengths, we find an elongation of $r(\text{Ni–O1})$ and $r(\text{Ni–O2})$ with adsorption of the first alkene molecule (1.74–1.82 and 1.74–1.81 Å at L1 and L2, respectively) as a consequence of the interactions of ethylene molecule with the active sites. This lengthening was intensified when the second adsorbate molecule interacted with the active site (1.80–1.95 and 1.79–1.95 Å at L1 and L2, respectively). Notably, the structural data were very similar with the two methods. Regarding the structural properties of the gas-phase molecule, the calculated length of $r(\text{C=C})$ was 1.33 or 1.32 Å at L1 or L2. Furthermore, the corresponding values of $\theta(\text{H–C–C})$ were 121.8° and 121.9° at L1 and L2, respectively. These data were in good agreement with the experimental estimates of 1.337 Å and 121.4° [4], respectively.

Also shown in Table S2 are the values of $r(\text{C}=\text{C})$ in the adsorbed alkene molecules which were lengthened by 0.04–0.06 and 0.03–0.04 Å after the consecutive adsorption of ethylene molecules. Meanwhile, regardless of the method employed, the corresponding H–C–H and H–C–C angles wavered around the initial gas-phase values of 116.3° and 121.9°, respectively (not shown here for the sake of conciseness). The length of the formed Ni–C bonds ranged from 2.00 to 2.09 Å and from 2.13 to 2.31 Å at L2 for the monomeric and dimeric adsorption modes, respectively. As it is clear, the ethylene molecules stabilized slightly farther from the surface in the dimeric mode with less changes in $r(\text{C}=\text{C})$ when compared to the monomeric adsorption stage. In fact, the partial flow of electrons from the ethylene molecules to the NiMCM-41 surface caused the formation of the Ni–C bonds and the elongation and weakening of the C=C bond, i.e., the π complexation.

The O–Ni–O angles changed over different ranges depending upon the adsorption mode. Although the O–Ni–O angles did not change drastically upon the adsorption of the first adsorptive molecule (83.4–169.0° at L1 and 83.6–169.6° at L2), the dimeric adsorption led to decreased values of $\theta(\text{O–Ni–O})$ due to the steric hindrance of the adsorbed molecules around the Ni center: 82.2–110.1° at L1 and 82.5–109.8° at L2 with the largest alterations on 4T and 5T. Again, the structural features obtained with L1 matched the corresponding data with L2 reasonably.

QTAIM is useful in characterizing the bond critical points (BCPs) in the calculated geometries, e.g., in terms of shared or closed-shell interactions. The obtained topological data for the L1 level of theory have been tabulated in Table S3, with the corresponding L2 values given in Table S8. The results of ρ_{BCP} together with the positive values of $\nabla^2\rho_{\text{BCP}}$ and small values of $|\lambda_{1,2}|/|\lambda_3|$ represented electrostatic interactions between the nickel ion and the olefinic bond. The initial shared but polar nature of the Ni–O bonds remained unchanged except on the 4T and 5T sites on which the nickel–surface interactions became electrostatic upon the adsorption of ethylene molecule(s). Overall, the topological results of the two methods were very similar except that L2 presented slightly larger (absolute) values of electron density, Laplacian, and eigenvalues.

As evident in Table S3, the dimeric adsorption further increased slightly the electrostatic nature of the bonds with respect to the monomeric mode. The QTAIM analysis showed that the active sites could establish BCPs for both of ethylene molecules at the dimeric stage. The eigenvalues were also in agreement with the highest exothermicity of the formation of D2T sites. We note also different correlations between the obtained topological data. Fig. S1 shows an example correlation between ρ_{BCP} and $r(\text{Ni}-\text{C})$ for the monomeric adsorption of ethylene over NiMCM-41. Analogous relationships were found in the previous studies on other systems [5]. Further significant correlations within a 95% confidence interval are shown in Figs. S2–S5 for the monomeric and dimeric adsorption modes.

According to the frontier molecular orbital (FMO) theory and the definition of chemical hardness as $\eta = (E_{\text{LUMO}} - E_{\text{HOMO}})/2$, one can employ the energy gaps between the highest occupied molecular orbital (HOMO) and the lowest unoccupied molecular orbital (LUMO) energy levels of different structures to obtain insights on the reactivity [5]. As a reasonable assumption with respect to the size of the pores and guest molecules, the chemical reactivities in the present case will be free from the confinement effects normally contributing in microporous catalysts. As shown in Tables S4 and S9, both HOMO and LUMO levels only slightly stabilized and the HOMO–LUMO energy gaps of the adsorbed complexes were further slightly expanded upon reaction (2). We noted also that some linear correlations could be established between the FMO energy levels calculated by the two methods (see Fig. S6).

Considering the general trends of the HOMO–LUMO energy gaps ($\Delta E_{\text{HOMO-LUMO}}$) before and after adsorption of alkene, there was no regular changes apparent in the scatter of data. In any event, the largest and smallest HOMO–LUMO gaps in the final adsorption structures belonged to D2T and D5T (and further D4T), respectively, with the $\Delta E_{\text{HOMO-LUMO}}$ values of 4.22 and 3.11 (3.41) eV at the L1 level of theory; the corresponding values of $\Delta E_{\text{HOMO-LUMO}}$ at L2 were 4.89 and 3.62 (4.20) eV, respectively (see Table S4). However, one may note from a recent publication [6] that the L1 level of theory is more accurate than L2 for the prediction of the HOMO–LUMO gaps.

We note that the least and most reactive sites before the adsorption stages turned into the most (D2T) and least (D5T and D4T) thermodynamically favored adsorption

complexes, respectively (refer to the estimated thermodynamic data discussed previously). Concerning the further roles of the structures in the subsequent reactions, the chemical hardness increased in the order of D5T < D4T < D3T < D6T1 < D6T3 < D6T1 < D2T at the L1 level.

It is often argued that time-dependent (TD) DFT methods predict the HOMO–LUMO gaps more accurately than conventional DFT methods. Therefore, we made also calculations with TD-B3LYP [7] to evaluate the HOMO–LUMO gaps. As is evident in Table S12, the equivalent TDDFT method predicted lower band gaps while same trends were obtained with respect to the original method.

From a standpoint of ethylene activation, the importance of a dimeric adsorption of ethylene over the 2T site was twofold: first, it showed the highest spontaneity to form in a porous NiMCM-41 catalyst and, second, the corresponding complex obtained after the adsorption of ethylene molecules possessed the highest polarizability and reactivity to further participate in the metallacycle mechanism. At the same time, we note that the initial 2T-type NiMCM-41 active sites would be in a minority particularly compared to the more abundant 5T clusters considering both experimental evidences [8] and the catalyst preparation thermodynamics [1]. These altogether raise the possibility for the presence of a large number of nickel-incorporated sites with 5T and 4T structures mainly as spectators.

Also listed in Table S4 are the stretching frequencies of the C=C bond ($\nu_{C=C}$) for the optimized geometries following the well-documented literature. The obtained data ranged within 1515–1544 and 1549–1562 cm^{-1} at L1 for the monomeric and dimeric adsorption structures, respectively. Compared with the experimental band of 1441 cm^{-1} for ethylene adsorption in Ni-MCM-41 [8] and taking into account that the computations overestimated the respective magnitudes for a free molecule (*vide infra*), we can accept that reasonable agreement has been found between the theoretical values of $\nu_{C=C}$ and the experimental data. One may note, however, that anharmonic frequencies should be calculated if theoretical estimates closer to experimental fundamentals are sought. In general, the changes in the vibrational frequencies with respect to the gas-phase molecule were more pronounced in the case of monomeric adsorption than the dimeric mode.

Table S1. NBO partial charges of selected atoms and total adsorbate charges (Q) for the adsorption of C_2H_4 on NiMCM-41 at the M06/Def2-TZVP level of theory.

Cluster	Ni	O1	O2	Si1	Si2	=C1a	=C1b	=C2a	=C2b	Q_1	Q_2
M2T	0.739	-0.949	-1.014	2.372	—	-0.420	-0.425	—	—	0.059	—
M3T	0.806	-1.090	-1.040	2.444	2.452	-0.384	-0.393	—	—	0.136	—
M4T	0.796	-1.122	-1.080	2.440	2.434	-0.332	-0.361	—	—	0.239	—
M5T	0.845	-1.106	-1.109	2.448	2.430	-0.359	-0.352	—	—	0.218	—
M6T1	0.832	-1.007	-1.101	2.447	2.474	-0.408	-0.399	—	—	0.094	—
M6T2	0.882	-1.007	-1.155	2.457	2.458	-0.390	-0.402	—	—	0.130	—
M6T3	0.825	-1.123	-1.006	2.465	2.443	-0.408	-0.390	—	—	0.123	—
D2T	0.490	-1.011	-1.009	2.391	—	-0.366	-0.352	-0.345	-0.372	0.178	0.179
D3T	0.621	-1.103	-1.117	2.452	2.469	-0.324	-0.374	-0.361	-0.334	0.211	0.209
D4T	0.698	-1.190	-1.125	2.459	2.465	-0.370	-0.315	-0.308	-0.365	0.226	0.243
D5T	0.718	-1.097	-1.186	2.457	2.455	-0.339	-0.356	-0.363	-0.330	0.224	0.214
D6T1	0.631	-1.086	-1.088	2.469	2.461	-0.330	-0.371	-0.370	-0.335	0.192	0.182
D6T2	0.660	-1.092	-1.110	2.466	2.461	-0.323	-0.366	-0.388	-0.340	0.220	0.189
D6T3	0.642	-1.113	-1.076	2.461	2.449	-0.320	-0.390	-0.383	-0.333	0.206	0.194

Table S2. Selected bonds lengths (Å) and interbond angles (in degrees) for different optimized cluster models at the M06/Def2-TZVP level of theory.

Cluster	Bond lengths								Angles
	Ni–O1	Ni–O2	Ni–C1a	Ni–C1b	Ni–C2a	Ni–C2b	C1a=C1b	C2a=C2b	O1–Ni–O2
M2T	1.79	1.77	2.06	2.06	—	—	1.36	—	83.6
M3T	1.78	1.81	2.08	2.09	—	—	1.36	—	113.7
M4T	1.80	1.80	2.01	2.01	—	—	1.38	—	169.6
M5T	1.77	1.80	2.01	2.01	—	—	1.38	—	164.9
M6T1	1.77	1.74	2.06	2.08	—	—	1.36	—	103.8
M6T2	1.76	1.76	2.08	2.08	—	—	1.36	—	102.6
M6T3	1.74	1.76	2.06	2.07	—	—	1.36	—	104.9
D2T	1.82	1.82	2.14	2.14	2.14	2.14	1.35	1.35	82.5
D3T	1.87	1.87	2.16	2.16	2.18	2.17	1.35	1.35	104.2
D4T	1.94	1.92	2.18	2.19	2.19	2.18	1.35	1.35	107.6
D5T	1.87	1.95	2.13	2.18	2.23	2.19	1.36	1.35	109.8
D6T1	1.79	1.80	2.17	2.17	2.16	2.16	1.35	1.35	96.3
D6T2	1.80	1.85	2.21	2.21	2.15	2.13	1.35	1.36	93.4
D6T3	1.81	1.85	2.16	2.18	2.17	2.14	1.35	1.35	91.2

Table S3. QTAIM data for the bond critical points obtained at the B3LYP/6-311+G* level of theory.

Cluster	BCP	ρ	λ_1	λ_2	λ_3	$\nabla^2\rho$
M2T	Ni-O1	0.133	-0.211	-0.209	0.971	0.551
	Ni-O2	0.139	-0.236	-0.215	1.105	0.654
	Ni-C1	0.084	-0.093	-0.030	0.357	0.234
M3T	Ni-O1	0.133	-0.227	-0.220	1.168	0.720
	Ni-O2	0.124	-0.185	-0.176	0.919	0.559
	Ni-C1	0.080	-0.086	-0.022	0.336	0.229
M4T	Ni-O1	0.124	-0.167	-0.165	1.004	0.672
	Ni-O2	0.127	-0.173	-0.171	0.993	0.649
	Ni-C1	0.095	-0.119	-0.031	0.383	0.233
M5T	Ni-O1	0.135	-0.196	-0.189	1.147	0.762
	Ni-O2	0.124	-0.169	-0.165	1.002	0.668
	Ni-C1	0.096	-0.120	-0.033	0.387	0.235
M6T1	Ni-O1	0.141	-0.225	-0.211	1.081	0.644
	Ni-O2	0.148	-0.257	-0.253	1.348	0.839
	Ni-C1	0.082	-0.088	-0.026	0.344	0.230
M6T2	Ni-O1	0.141	-0.224	-0.212	1.070	0.634
	Ni-O2	0.139	-0.230	-0.220	1.227	0.778
	Ni-C1	0.081	-0.088	-0.025	0.332	0.220
M6T3	Ni-O1	0.144	-0.255	-0.250	1.363	0.858
	Ni-O2	0.140	-0.226	-0.215	1.085	0.645
	Ni-C1	0.086	-0.095	-0.034	0.360	0.231

Table S3. Continued.

Cluster	BCP	ρ	λ_1	λ_2	λ_3	$\nabla^2\rho$
D2T	Ni–O1	0.122	–0.191	–0.180	0.913	0.542
	Ni–O2	0.122	–0.192	–0.181	0.915	0.542
	Ni–C1	0.069	–0.068	–0.011	0.286	0.206
	Ni–C2	0.069	–0.068	–0.011	0.286	0.207
D3T	Ni–O1	0.105	–0.151	–0.140	0.794	0.503
	Ni–O2	0.107	–0.154	–0.146	0.819	0.519
	Ni–C1	0.066	–0.066	–0.020	0.260	0.174
	Ni–C2	0.064	–0.062	–0.018	0.251	0.172
D4T	Ni–O1	0.087	–0.117	–0.111	0.686	0.458
	Ni–O2	0.098	–0.137	–0.131	0.758	0.491
	Ni–C1	0.062	–0.061	–0.022	0.237	0.155
	Ni–C2	0.066	–0.068	–0.020	0.256	0.168
D5T	Ni–O1	0.107	–0.155	–0.144	0.857	0.558
	Ni–O2	0.087	–0.120	–0.116	0.684	0.448
	Ni–C1	0.074	–0.081	–0.039	0.287	0.167
	Ni–C2	0.057	–0.056	–0.031	0.217	0.130
D6T1	Ni–O1	0.127	–0.200	–0.182	1.018	0.636
	Ni–O2	0.123	–0.193	–0.174	0.999	0.632
	Ni–C1	0.064	–0.061	–0.015	0.256	0.181
	Ni–C2	0.063	–0.060	–0.016	0.254	0.179
D6T2	Ni–O1	0.125	–0.195	–0.182	1.030	0.652
	Ni–O2	0.109	–0.161	–0.145	0.882	0.576
	Ni–C1	0.058	–0.055	–0.022	0.221	0.145
	Ni–C2	0.073	–0.077	–0.033	0.288	0.179
D6T3	Ni–O1	0.120	–0.185	–0.168	0.975	0.622
	Ni–O2	0.114	–0.172	–0.155	0.872	0.546
	Ni–C1	0.066	–0.067	–0.032	0.256	0.157
	Ni–C2	0.068	–0.069	–0.035	0.263	0.159

Table S4. HOMO–LUMO energy gaps ($\Delta E_{\text{HOMO-LUMO}}$) and C=C stretching frequencies (cm^{-1}) of the olefinic bond ($\nu_{\text{C=C}}$) for the investigated clusters at the B3LYP/6-311+G* and M06/Def2-TZVP levels of theory.

Cluster	$\Delta E_{\text{HOMO-LUMO}}$ (eV)		$\nu_{\text{C1=C1}}$		$\nu_{\text{C2=C2}}$	
	L1	L2	L1	L2	L1	L2
M2T	3.46	4.16	1542	1516	—	—
M3T	3.21	3.85	1544	1520	—	—
M4T	3.51	4.16	1515	1481	—	—
M5T	3.74	4.32	1516	1488	—	—
M6T1	3.32	4.02	1541	1518	—	—
M6T2	3.20	3.90	1544	1523	—	—
M6T3	3.35	3.91	1541	1519	—	—
D2T	4.22	4.89	1550	1530	1556	1537
D3T	3.69	4.25	1549	1527	1556	1532
D4T	3.41	4.02	1549	1527	1555	1532
D5T	3.11	3.62	1552	1528	1560	1536
D6T1	3.84	4.40	1550	1530	1557	1536
D6T2	3.72	4.41	1549	1531	1562	1538
D6T3	3.78	4.44	1556	1534	1561	1540

Table S5. NBO partial charges of selected atoms and total adsorbate charges (Q) for the adsorption of C_2H_4 on NiMCM-41 at the B3LYP/6-311+G* level of theory.

Cluster	Ni	O1	O2	Si1	Si2	=C1a	=C1b	=C2a	=C2b	Q_1	Q_2
M2T	0.820	-0.970	-1.033	2.366	—	-0.425	-0.431	—	—	0.022	—
M3T	0.886	-1.106	-1.057	2.443	2.448	-0.390	-0.401	—	—	0.095	—
M4T	0.863	-1.145	-1.104	2.432	2.432	-0.327	-0.364	—	—	0.220	—
M5T	0.906	-1.126	-1.132	2.444	2.418	-0.367	-0.338	—	—	0.196	—
M6T1	0.911	-1.041	-1.112	2.449	2.466	-0.415	-0.402	—	—	0.055	—
M6T2	0.966	-1.027	-1.173	2.454	2.452	-0.405	-0.405	—	—	0.082	—
M6T3	0.900	-1.129	-1.030	2.456	2.436	-0.415	-0.393	—	—	0.080	—
D2T	0.591	-1.034	-1.032	2.381	—	-0.357	-0.365	-0.357	-0.364	0.155	0.155
D3T	0.720	-1.126	-1.134	2.448	2.459	-0.338	-0.370	-0.359	-0.343	0.181	0.182
D4T	0.794	-1.221	-1.135	2.450	2.461	-0.368	-0.323	-0.325	-0.360	0.204	0.217
D5T	0.812	-1.111	-1.205	2.446	2.441	-0.345	-0.355	-0.363	-0.336	0.191	0.188
D6T1	0.742	-1.104	-1.119	2.460	2.457	-0.348	-0.362	-0.364	-0.350	0.161	0.154
D6T2	0.768	-1.116	-1.122	2.461	2.451	-0.339	-0.364	-0.392	-0.351	0.188	0.149
D6T3	0.758	-1.136	-1.104	2.454	2.441	-0.330	-0.393	-0.388	-0.337	0.170	0.157

Table S6. Mulliken atomic charges of selected atoms and total adsorbate charges (Q) for the adsorption of C_2H_4 on NiMCM-41 at the M06/Def2-TZVP level of theory.

Cluster	Ni	O1	O2	Si1	Si2	=C1a	=C1b	=C2a	=C2b
M2T	0.385	-0.495	-0.495	0.895	—	-0.178	-0.185	—	—
M3T	0.343	-0.527	-0.497	0.851	0.839	-0.175	-0.131	—	—
M4T	0.301	-0.453	-0.466	0.770	0.794	-0.111	-0.158	—	—
M5T	0.354	-0.440	-0.468	0.726	0.764	-0.199	-0.117	—	—
M6T1	0.383	-0.458	-0.429	0.697	0.697	-0.214	-0.116	—	—
M6T2	0.332	-0.428	-0.417	0.742	0.769	-0.210	-0.114	—	—
M6T3	0.359	-0.388	-0.439	0.730	0.766	-0.254	-0.097	—	—
D2T	0.155	-0.500	-0.500	0.867	—	-0.131	-0.168	-0.167	-0.132
D3T	0.164	-0.518	-0.490	0.822	0.818	-0.191	-0.104	-0.119	-0.177
D4T	0.272	-0.482	-0.503	0.724	0.778	-0.170	-0.165	-0.188	-0.110
D5T	0.243	-0.417	-0.504	0.715	0.756	-0.190	-0.126	-0.153	-0.174
D6T1	0.164	-0.412	-0.428	0.685	0.703	-0.188	-0.107	-0.097	-0.191
D6T2	0.153	-0.381	-0.362	0.694	0.706	-0.247	-0.074	-0.117	-0.200
D6T3	0.173	-0.328	-0.426	0.677	0.741	-0.156	-0.096	-0.221	-0.122

Table S7. Selected bonds lengths (Å) and interbond angles (in degrees) for different optimized cluster models at the B3LYP/6-31+G* level of theory.

Cluster	Bond lengths							Angles	
	Ni–O1	Ni–O2	Ni–C1a	Ni–C1b	Ni–C2a	Ni–C2b	C1a=C1b	C2a=C2b	O1–Ni–O2
M2T	1.81	1.79	2.07	2.07	—	—	1.38	—	83.4
M3T	1.79	1.82	2.09	2.09	—	—	1.37	—	112.1
M4T	1.80	1.80	2.01	2.01	—	—	1.39	—	169.0
M5T	1.77	1.81	2.01	2.00	—	—	1.39	—	164.5
M6T1	1.77	1.74	2.08	2.08	—	—	1.37	—	105.0
M6T2	1.77	1.76	2.09	2.09	—	—	1.37	—	102.0
M6T3	1.75	1.77	2.06	2.07	—	—	1.38	—	104.8
D2T	1.84	1.84	2.16	2.16	2.16	2.16	1.37	1.37	82.2
D3T	1.88	1.88	2.18	2.19	2.21	2.20	1.37	1.36	103.4
D4T	1.94	1.90	2.23	2.21	2.18	2.20	1.36	1.37	108.9
D5T	1.86	1.95	2.13	2.18	2.31	2.24	1.37	1.36	110.1
D6T1	1.80	1.81	2.20	2.20	2.20	2.20	1.36	1.36	96.4
D6T2	1.80	1.85	2.24	2.27	2.16	2.13	1.36	1.37	93.0
D6T3	1.82	1.85	2.18	2.22	2.22	2.16	1.37	1.36	91.5

Table S8. QTAIM data for the bond critical points obtained at the M06/Def2-TZVP level of theory.

Cluster	BCP	ρ	λ_1	λ_2	λ_3	$\nabla^2\rho$
M2T	Ni-O1	0.139	-0.219	-0.207	0.970	0.544
	Ni-O2	0.144	-0.236	-0.206	1.085	0.643
	Ni-C1	0.085	-0.087	-0.031	0.358	0.241
M3T	Ni-O1	0.138	-0.236	-0.224	1.166	0.706
	Ni-O2	0.128	-0.186	-0.170	0.914	0.557
	Ni-C1	0.081	-0.081	-0.022	0.334	0.231
M4T	Ni-O1	0.125	-0.156	-0.153	0.986	0.677
	Ni-O2	0.129	-0.163	-0.160	0.985	0.662
	Ni-C1	0.095	-0.114	-0.027	0.387	0.246
M5T	Ni-O1	0.135	-0.185	-0.176	1.121	0.760
	Ni-O2	0.126	-0.159	-0.155	0.981	0.667
	Ni-C1	0.095	-0.114	-0.028	0.387	0.244
M6T1	Ni-O1	0.143	-0.221	-0.203	1.066	0.642
	Ni-O2	0.151	-0.261	-0.257	1.359	0.842
	Ni-C1	0.085	-0.087	-0.038	0.353	0.228
M6T2	Ni-O1	0.144	-0.223	-0.203	1.086	0.660
	Ni-O2	0.142	-0.232	-0.225	1.238	0.781
	Ni-C1	0.082	-0.081	-0.019	0.335	0.235
M6T3	Ni-O1	0.149	-0.269	-0.257	1.384	0.858
	Ni-O2	0.143	-0.221	-0.206	1.084	0.657
	Ni-C1	0.086	-0.092	-0.036	0.359	0.232

Table S8. Continued.

Cluster	BCP	ρ	λ_1	λ_2	λ_3	$\nabla^2\rho$
D2T	Ni-O1	0.128	-0.196	-0.176	0.906	0.534
	Ni-O2	0.128	-0.197	-0.177	0.910	0.536
	Ni-C1	0.072	-0.067	-0.009	0.299	0.223
	Ni-C2	0.072	-0.067	-0.010	0.300	0.223
D3T	Ni-O1	0.108	-0.152	-0.139	0.769	0.479
	Ni-O2	0.109	-0.154	-0.142	0.791	0.494
	Ni-C1	0.070	-0.068	-0.016	0.280	0.195
	Ni-C2	0.069	-0.065	-0.015	0.273	0.193
D4T	Ni-O1	0.090	-0.119	-0.114	0.647	0.414
	Ni-O2	0.097	-0.130	-0.124	0.680	0.426
	Ni-C1	0.067	-0.060	-0.003	0.259	0.196
	Ni-C2	0.068	-0.063	-0.006	0.259	0.191
D5T	Ni-O1	0.106	-0.151	-0.139	0.796	0.506
	Ni-O2	0.089	-0.121	-0.115	0.633	0.396
	Ni-C1	0.074	-0.077	-0.034	0.293	0.182
	Ni-C2	0.065	-0.064	-0.029	0.258	0.165
D6T1	Ni-O1	0.130	-0.200	-0.177	1.030	0.653
	Ni-O2	0.127	-0.193	-0.171	0.997	0.633
	Ni-C1	0.069	-0.066	-0.016	0.277	0.196
	Ni-C2	0.070	-0.067	-0.018	0.286	0.200
D6T2	Ni-O1	0.129	-0.196	-0.178	1.031	0.657
	Ni-O2	0.110	-0.156	-0.135	0.838	0.546
	Ni-C1	0.064	-0.059	-0.013	0.249	0.177
	Ni-C2	0.074	-0.073	-0.025	0.296	0.198
D6T3	Ni-O1	0.124	-0.186	-0.164	0.971	0.621
	Ni-O2	0.116	-0.168	-0.148	0.842	0.526
	Ni-C1	0.070	-0.068	-0.023	0.275	0.185
	Ni-C2	0.072	-0.071	-0.028	0.284	0.186

Table S9. Calculated HOMO and LUMO energy levels at L1 and L2.

Cluster	E_{HOMO} (eV)		E_{LUMO} (eV)	
	L1	L2	L1	L2
M2T	-6.82	-7.11	-3.36	-2.95
M3T	-6.90	-7.24	-3.69	-3.39
M4T	-7.03	-7.19	-3.52	-3.03
M5T	-7.05	-7.17	-3.31	-2.85
M6T1	-6.55	-6.96	-3.23	-2.94
M6T2	-6.50	-6.91	-3.30	-3.01
M6T3	-6.75	-7.03	-3.40	-3.12
D2T	-6.53	-6.82	-2.31	-1.93
D3T	-6.57	-6.86	-2.88	-2.61
D4T	-6.96	-7.09	-3.55	-3.07
D5T	-6.79	-6.94	-3.68	-3.32
D6T1	-6.32	-6.66	-2.48	-2.26
D6T2	-6.14	-6.55	-2.42	-2.14
D6T3	-6.46	-6.74	-2.67	-2.30

Table S10. The bond length of C=C (Å) for free ethylene molecules in gas phase at L1 and L2.

	Bond length	
	L1	L2
C ₂ H ₄	1.33	1.32

Table S11. The enthalpy (kcal/mol), entropy (cal/mol/K), and Gibbs free energy (kcal/mol) changes upon adsorption of ethylene at 393 K (M06/Def2-TZVP level of theory).

Cluster	ΔH_{ads}	ΔS_{ads}	ΔG_{ads}
M2T	-32.2	-37.8	-17.3
M4T	-35.4	-41.5	-19.1
M5T	-32.0	-37.1	-17.4
D2T	-54.2	-77.4	-23.7
D4T	-24.2	-77.6	6.3
D5T	-12.4	-72.0	15.9
Ni-SSZ-24 [9]	-28.7	-39.9	-12.9

Table S12. The HOMO–LUMO gaps (eV) for the optimized clusters at the B3LYP/6-311+G* level of theory.

Cluster	E_g
M2T	1.14
M3T	0.69
M4T	1.11
M5T	1.25
M6T1	0.83
M6T2	0.70
M6T3	0.72
D2T	2.14
D3T	1.56
D4T	1.15
D5T	0.86
D6T1	1.64
D6T2	1.49
D6T3	1.55

Table S13. Second-order perturbation theory analysis of Fock matrix in NBO basis for π -bonding between ethylene molecules and active sites at the M06/Def2-TZVPD level of theory.

Cluster	Donor (i)	Acceptor (j)	kcal/mol	a.u.	a.u.
			$E(2)^a$	$E(j)-E(i)^b$	$F(i, j)^c$
M2T	C1a=C1b	Ni	7.70	1.19	0.089
M3T	C1a=C1b	Ni	7.35	1.23	0.088
M4T	C1a=C1b	Ni	8.90	1.03	0.087
M5T	C1a=C1b	Ni	13.93	1.15	0.119
M6T1	C1a=C1b	Ni	8.89	1.14	0.094
M6T2	C1a=C1b	Ni	8.01	1.22	0.092
M6T3	C1a=C1b	Ni	9.52	1.14	0.097
D2T	C1a=C1b	Ni	56.87	0.70	0.181
	C2a=C2b	Ni	59.09	0.70	0.185
D3T	C1a=C1b	Ni	5.12	1.32	0.078
	C2a=C2b	Ni	5.18	1.12	0.071
D4T	C1a=C1b	Ni	5.36	1.13	0.073
	C2a=C2b	Ni	5.02	1.32	0.077
D5T	C1a=C1b	Ni	5.10	1.29	0.076
	C2a=C2b	Ni	4.49	1.13	0.067
D6T1	C1a=C1b	Ni	4.59	1.1	0.067
	C2a=C2b	Ni	4.63	1.09	0.067
D6T2	C1a=C1b	Ni	4.03	1.13	0.063
	C2a=C2b	Ni	5.23	1.11	0.072
D6T3	C1a=C1b	Ni	5.44	1.14	0.074
	C2a=C2b	Ni	5.40	1.24	0.077

^a Energy of hyperconjugative interactions

^b Energy difference between donor and acceptor i and j NBO orbitals

^c $F(i, j)$ is the Fock matrix element between i and j NBO orbitals

Table S14. NHO directionality and the bending angles (deviations from line of nuclear centers) of the adsorbed ethylene on different active sites at the M06/Def2-TZVP level of theory.

Cluster	Bond	Line of Center		Hybrid 1			Hybride 2		
		θ (in degree)	φ (in degree)	θ (in degree)	φ (in degree)	Dev.	θ (in degree)	φ (in degree)	Dev.
M2T	π (C1a=C2a)	88.5	91.1	96.5	76.9	16.3	101.4	289.1	20.4
M3T	π (C1a=C2a)	152.8	124.0	138.5	147.7	19.4	21.6	257.4	19.5
M4T	π (C1a=C2a)	161.1	270.0	144.7	268.9	16.4	2.7	105.3	16.4
M5T	π (C1a=C2a)	58.5	76.4	44.1	72.0	14.8	105.5	260.0	16.4
M6T1	π (C1a=C2a)	116.6	48.6	123.6	65.7	16.4	74.5	210.2	20.4
M6T2	π (C1a=C2a)	103.5	70.1	118.0	77.6	16.1	94.2	241.9	19.5
M6T3	π (C1a=C2a)	128.7	108.4	139.4	91.2	16.3	66.8	303.4	20.1
D2T	π (C1a=C2a)	173.3	297.7	103.3	56.4	79.9	83.2	58.4	79.8
	π (C1b=C2b)	8.0	45.5	78.3	303.9	80.0	98.4	302.2	79.8
D3T	π (C1a=C2a)	157.1	43.8	148.4	81.8	19.0	27.0	179.1	18.9
	π (C1b=C2b)	18.3	282.6	33.1	254.2	18.9	163.3	168.7	18.9
D4T	π (C1a=C2a)	24.8	269.2	18.0	221.9	18.0	140.8	110.3	18.0
	π (C1b=C2b)	40.9	272	32.9	298.2	17.5	127.1	74.9	17.2
D5T	π (C1a=C2a)	43.4	37.6	31.1	16.0	17.8	121.9	230.6	17.8
	π (C1b=C2b)	13.5	38.5	15.4	115.9	18.0	152.3	184.7	17.9
D6T1	π (C1a=C2a)	140.0	218.4	138.8	248.4	19.4	46.3	11.4	19.4
	π (C1b=C2b)	24.4	63.1	44.1	62.6	19.8	175.3	250.4	19.7
D6T2	π (C1a=C2a)	108.1	48.8	120.3	63.1	17.9	85.0	216.6	17.6
	π (C1b=C2b)	51.4	220.7	64.1	238.4	19.6	137.9	16.9	19.5
D6T3	π (C1a=C2a)	110.0	106.5	126.1	117.8	18.9	86.6	277.3	18.9
	π (C1b=C2b)	39.7	281.2	50.4	304.5	19.4	144.7	70.2	19.2

Table S15. Wiberg bond index matrix in the NAO basis calculated at M06/Def2-TZVP.

Cluster	Interatomic Distance	WBIs
M2T	Ni-C1a	0.335
	Ni-C2a	0.335
M3T	Ni-C1a	0.330
	Ni-C2a	0.327
M4T	Ni-C1a	0.433
	Ni-C2a	0.424
M5T	Ni-C1a	0.422
	Ni-C2a	0.432
M6T1	Ni-C1a	0.345
	Ni-C2a	0.343
M6T2	Ni-C1a	0.324
	Ni-C2a	0.334
M6T3	Ni-C1a	0.357
	Ni-C2a	0.356
D2T	Ni-C1a	0.313
	Ni-C2a	0.307
	Ni-C1b	0.306
	Ni-C2b	0.314
D3T	Ni-C1a	0.304
	Ni-C2a	0.323
	Ni-C1b	0.310
	Ni-C2b	0.296
D4T	Ni-C1a	0.315
	Ni-C2a	0.300
	Ni-C1b	0.305
	Ni-C2b	0.325
D5T	Ni-C1a	0.329
	Ni-C2a	0.333
	Ni-C1b	0.293
	Ni-C2b	0.285
D6T1	Ni-C1a	0.294
	Ni-C2a	0.317
	Ni-C1b	0.323
	Ni-C2b	0.302

Table S15. Wiberg bond index matrix in the NAO basis calculated at M06/Def2-TZVP.

Cluster	Interatomic Distance	WBIs
D6T2	Ni-C1a	0.285
	Ni-C2a	0.306
	Ni-C1b	0.334
	Ni-C2b	0.319
D6T3	Ni-C1a	0.273
	Ni-C2a	0.285
	Ni-C1b	0.291
	Ni-C2b	0.290

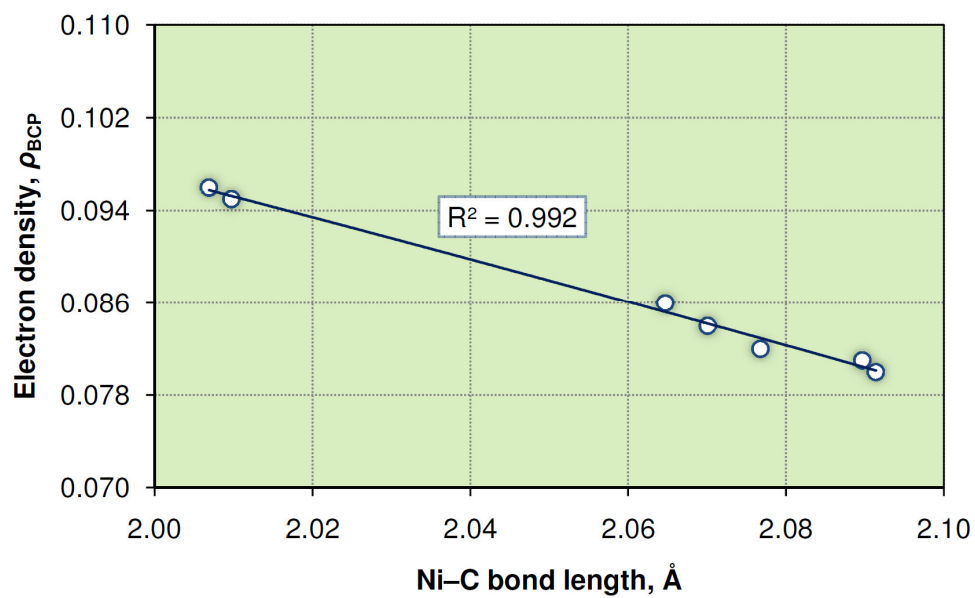


Figure S1. An example correlation found between the topological properties and the Ni-C distances for the monomeric adsorption of ethylene on NiMCM-41 at L1.

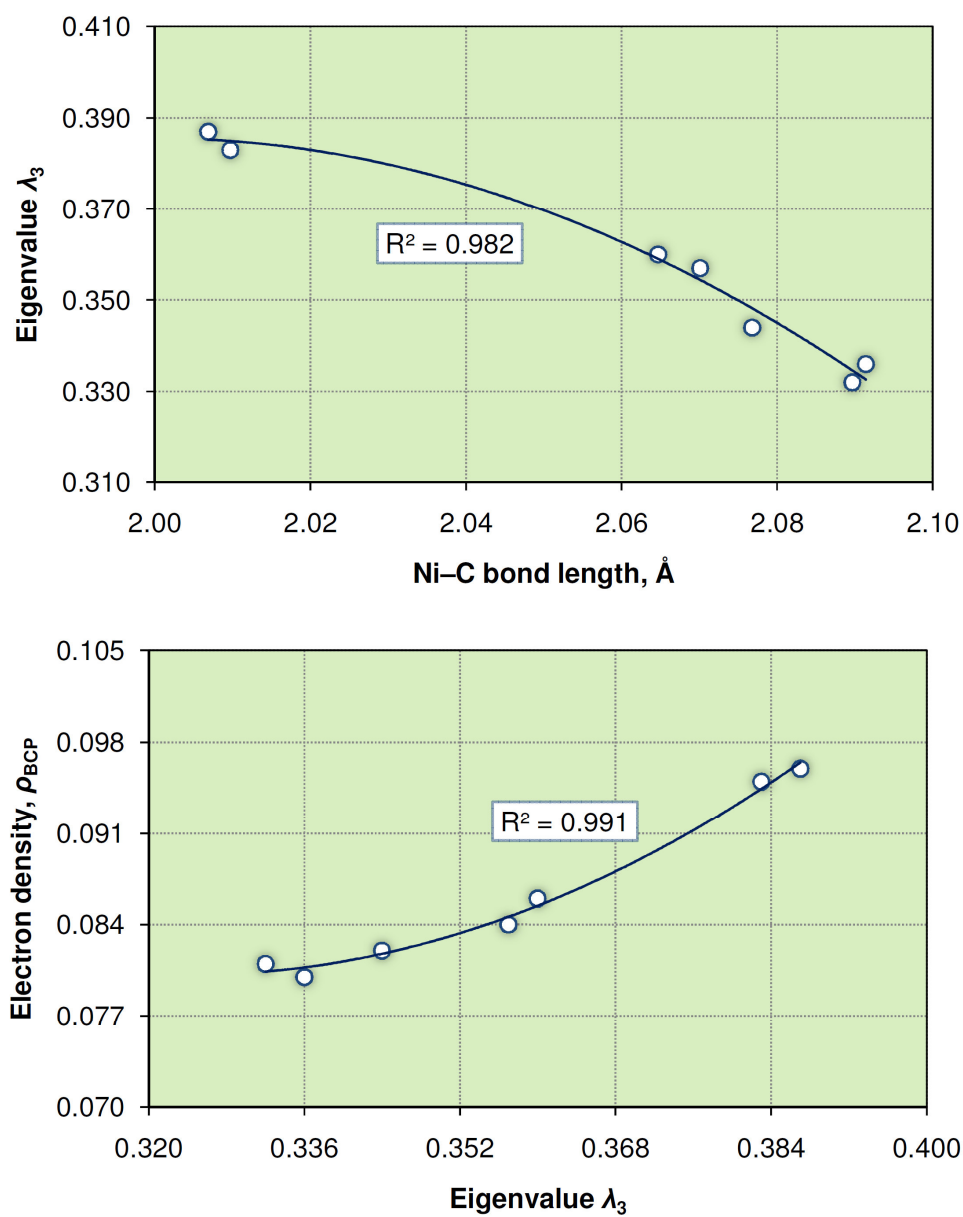


Figure S2. Significant correlations with confidence levels of 95% between the topological properties of the Ni-C bonds for the monomeric stage of ethylene adsorption on NiMCM-41 at the B3LYP/6-31+G* level.

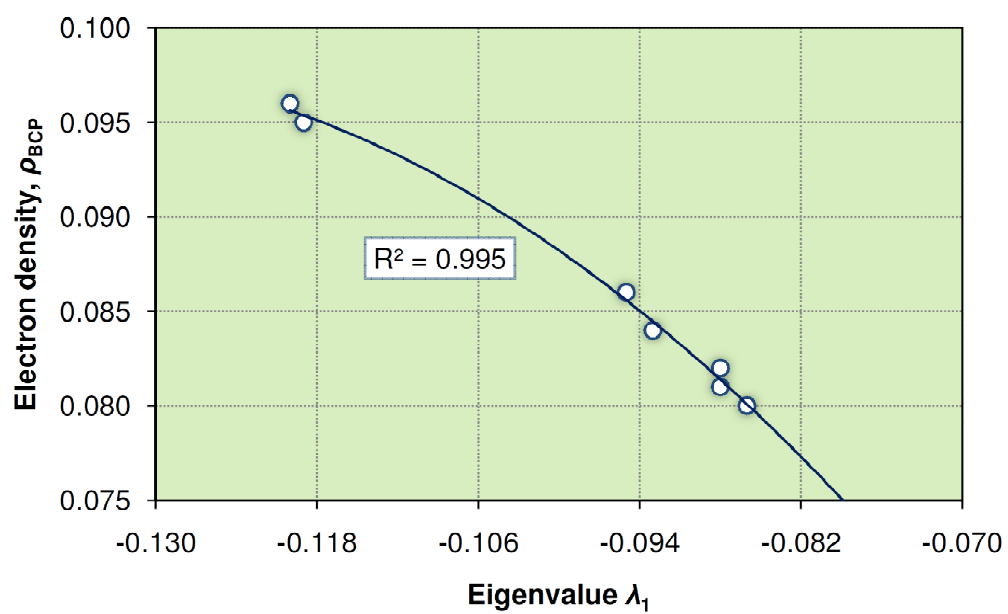


Figure S2. Continued.

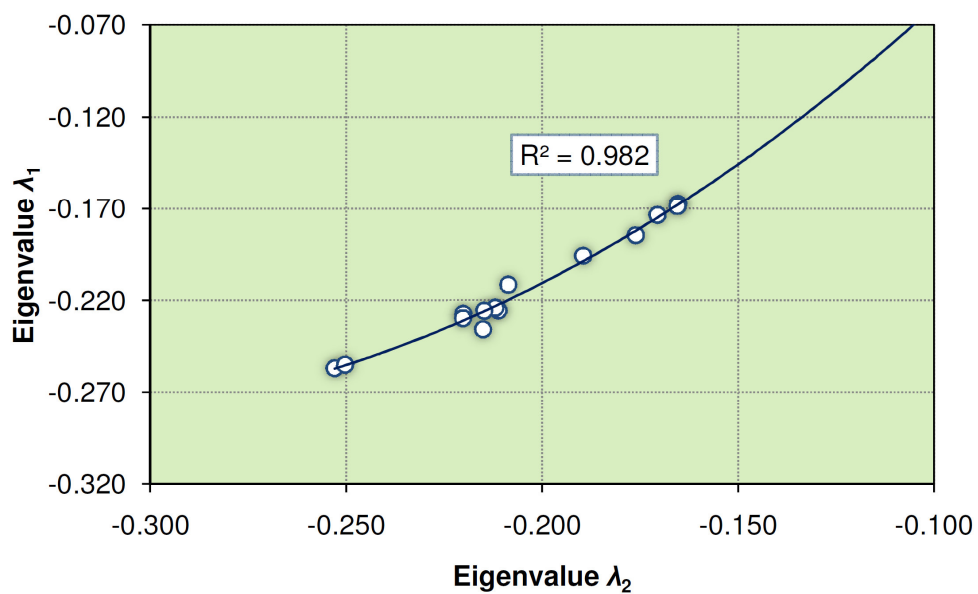


Figure S3. Significant correlations with confidence levels of 95% between the topological properties of the Ni–O bonds for the monomeric stage of ethylene adsorption on NiMCM-41 at the B3LYP/6-31+G* level.

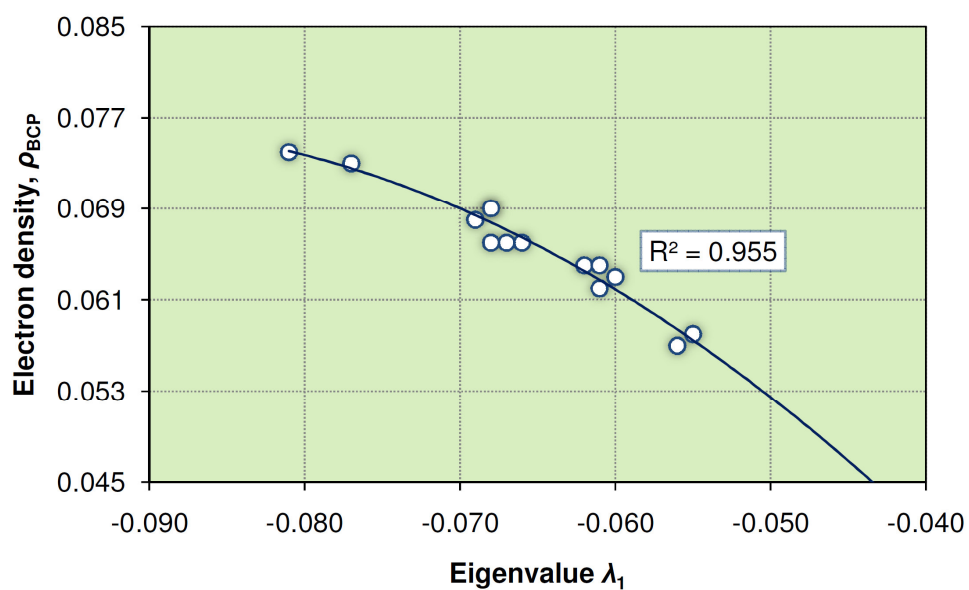


Figure S4. Significant correlations with confidence levels of 95% between the topological properties of the Ni–C bonds for the dimeric mode of ethylene adsorption on NiMCM-41 at the B3LYP/6-31+G* level.

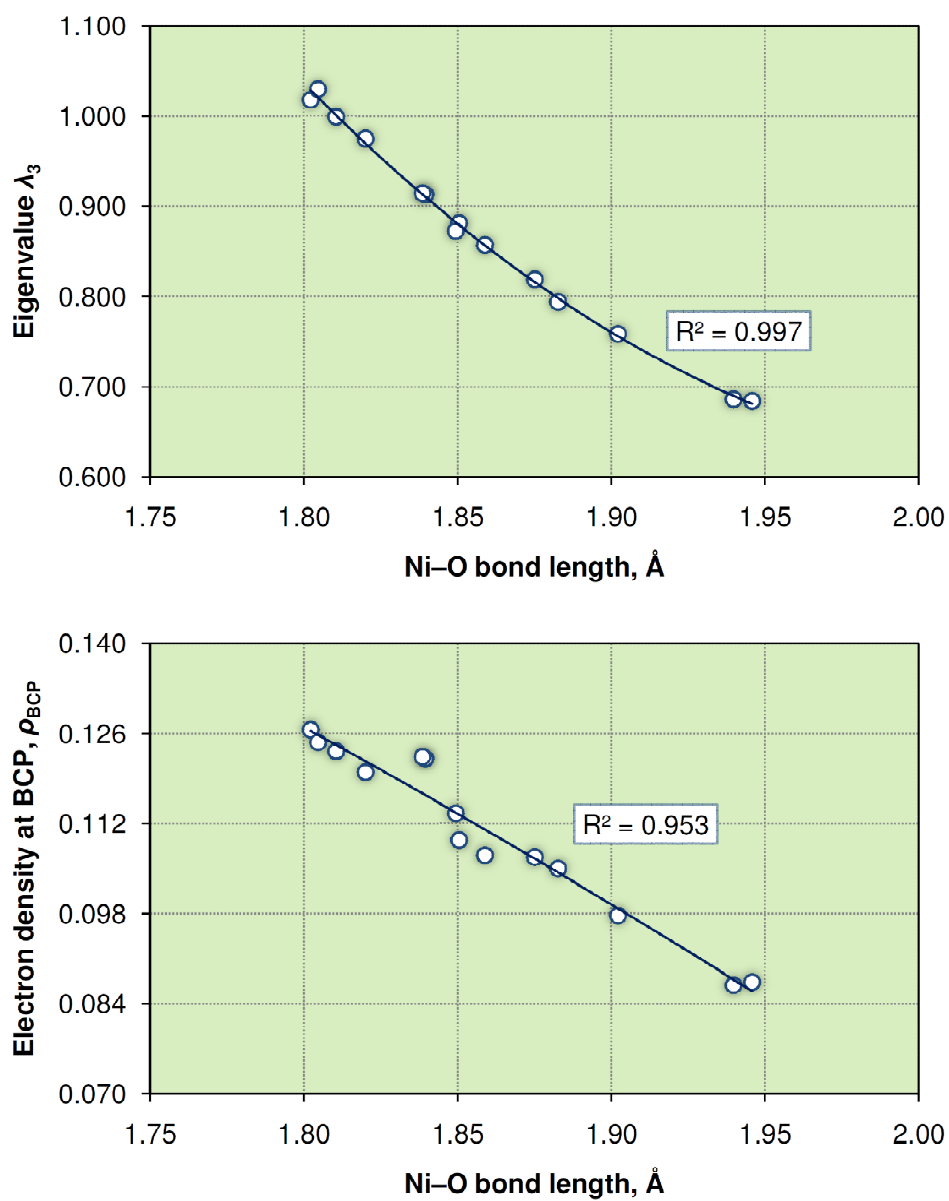


Figure S5. Significant correlations with confidence levels of 95% between the topological properties of the Ni-O bonds for the dimeric mode of ethylene adsorption on NiMCM-41 at the B3LYP/6-31+G* level.

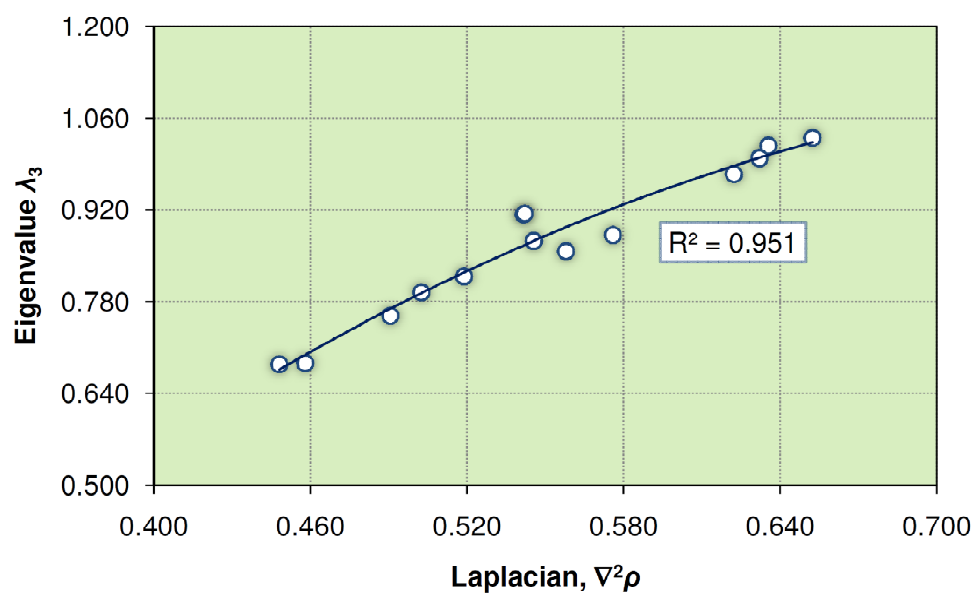
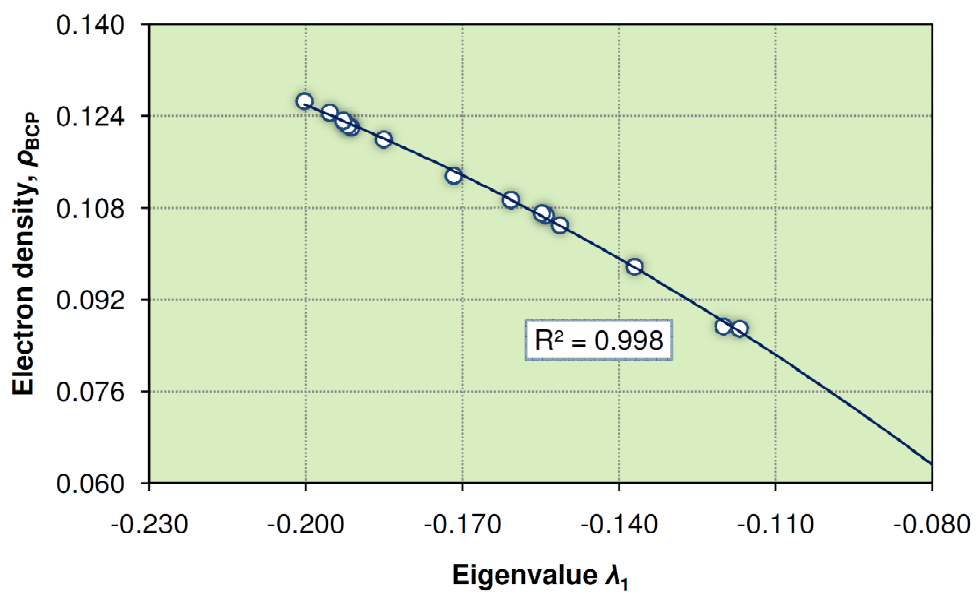


Figure S5. Continued.

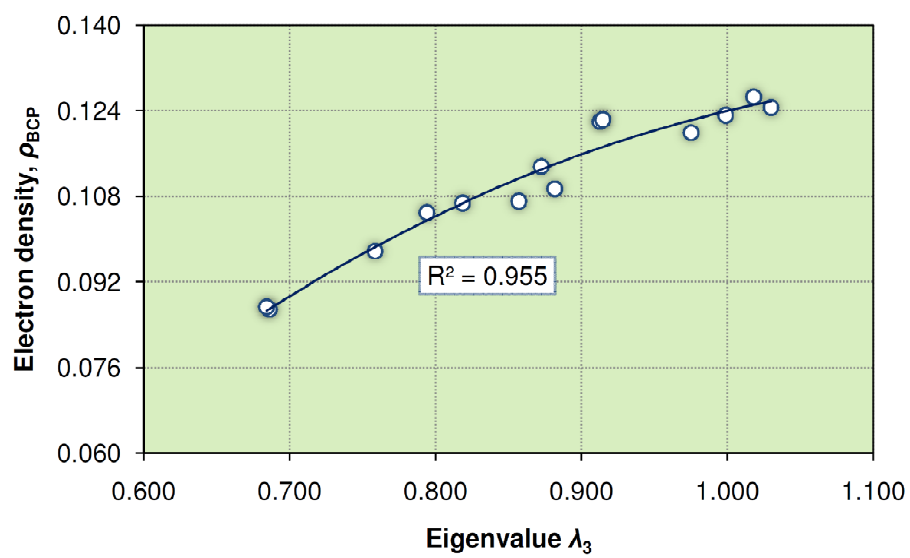
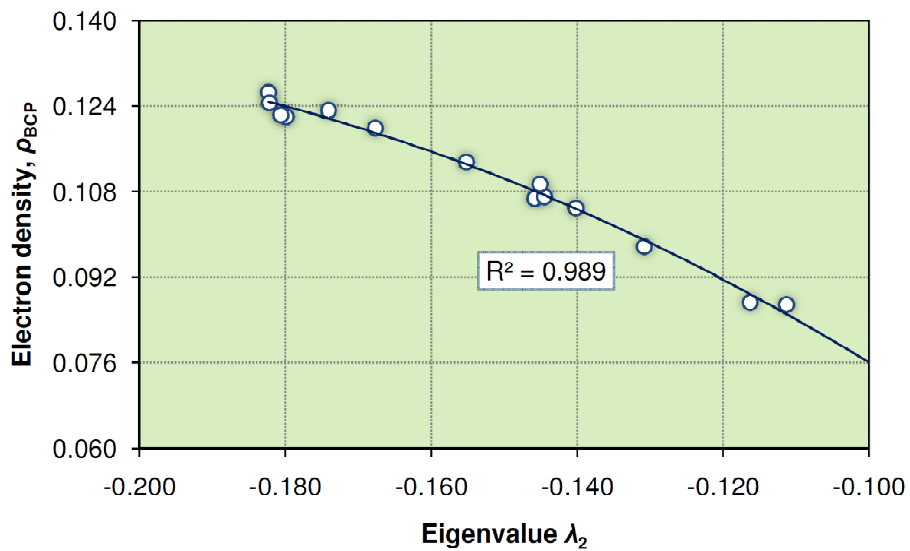


Figure S5. Continued.

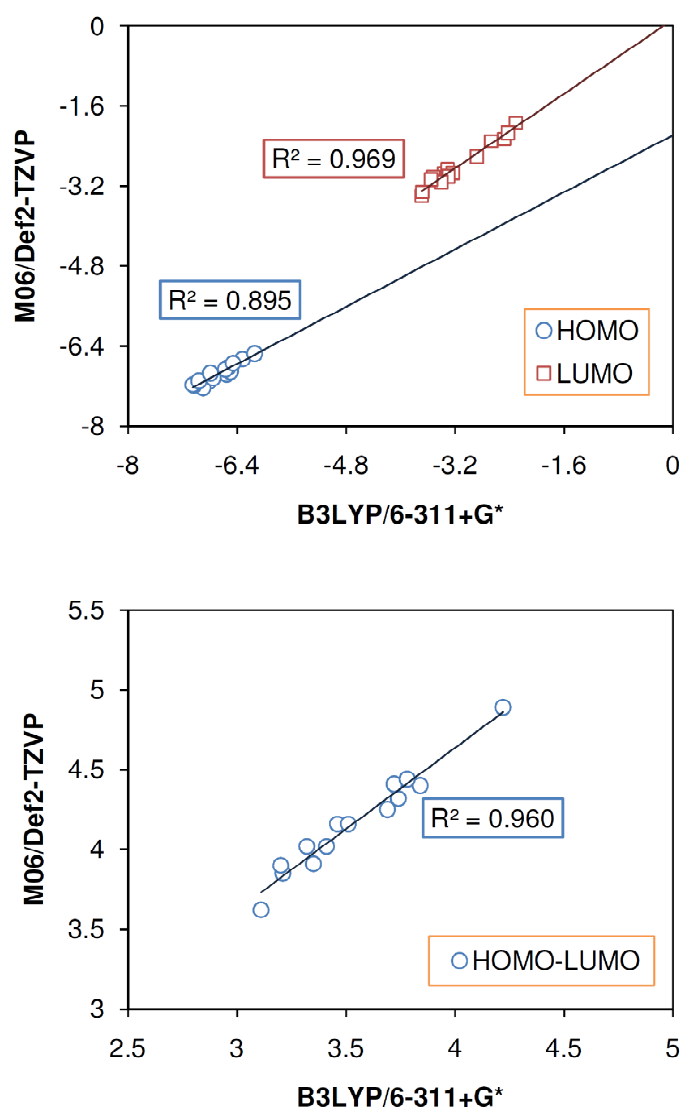


Figure S6. Linear correlations found between the HOMO and LUMO levels and HOMO-LUMO gaps obtained with the two methods.

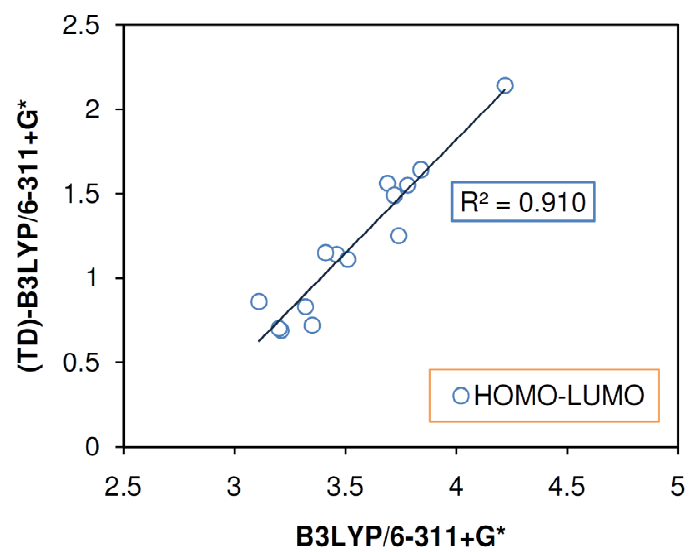


Figure S6. Continued.

References:

- [1] Balar, M.; Azizi, Z.; Ghashghaee, M., Theoretical identification of structural heterogeneities of divalent nickel active sites in NiMCM-41 nanoporous catalysts. *J. Nanostruct. Chem.* **2016**, *6* (4), 365–372, DOI: 10.1007/s40097-016-0208-z.
- [2] Yang, J. C.; Shul, Y. G.; Louis, C.; Che, M., In situ EXAFS study of the nucleation and crystal growth of Ni particles on SiO₂ support. *Catal. Today* **1998**, *44* (1–4), 315–325, DOI: [http://dx.doi.org/10.1016/S0920-5861\(98\)00205-3](http://dx.doi.org/10.1016/S0920-5861(98)00205-3).
- [3] Clause, O.; Bonneviot, L.; Che, M.; Dexpert, H., EXAFS characterization of the adsorbed state of Ni(II) ions in Ni/SiO₂ materials prepared by deposition-precipitation. *J. Catal.* **1991**, *130* (1), 21–28, DOI: [http://dx.doi.org/10.1016/0021-9517\(91\)90088-L](http://dx.doi.org/10.1016/0021-9517(91)90088-L).
- [4] Allen, H. C.; Plyler, E. K., The Structure of Ethylene from Infrared Spectra. *J. Am. Chem. Soc.* **1958**, *80* (11), 2673–2676, DOI: 10.1021/ja01544a021.
- [5] Ghambarian, M.; Azizi, Z.; Ghashghaee, M., Diversity of monomeric dioxo chromium species in Cr/silicalite-2 catalysts: A hybrid density functional study. *Comp. Mater. Sci.* **2016**, *118*, 147–154, DOI: 10.1016/j.commatsci.2016.03.009.
- [6] Medvedev, M. G.; Bushmarinov, I. S.; Sun, J.; Perdew, J. P.; Lyssenko, K. A., Density functional theory is straying from the path toward the exact functional. *Science* **2017**, *355* (6320), 49–52, DOI: 10.1126/science.aah5975.
- [7] Becke, A. D., Density-functional thermochemistry. III. The role of exact exchange. *J. Chem. Phys.* **1993**, *98* (7), 5648–5652, DOI: <http://dx.doi.org/10.1063/1.464913>.
- [8] Tanaka, M.; Itadani, A.; Kuroda, Y.; Iwamoto, M., Effect of pore size and nickel content of Ni-MCM-41 on catalytic activity for ethene dimerization and local structures of nickel ions. *J. Phys. Chem. C* **2012**, *116* (9), 5664–5672, DOI: 10.1021/jp2103066.
- [9] Brogaard, R. Y.; Olsbye, U., Ethene Oligomerization in Ni-Containing Zeolites: Theoretical Discrimination of Reaction Mechanisms. *ACS Catal.* **2016**, *6* (2), 1205–1214, DOI: 10.1021/acscatal.5b01957.